



Obesity-associated inflammation promotes angiogenesis and breast cancer via angiopoietin-like 4

Ryan Kolb^{1,2} · Paige Kluz^{1,3} · Zhen Wei Tan⁴ · Nicholas Borcharding^{1,5,6} · Nicholas Bormann⁷ · Ajaykumar Vishwakarma^{1,6} · Louis Balczak⁸ · Pengcheng Zhu⁴ · Brandon S.J. Davies⁹ · Françoise Gourronc¹⁰ · Ling-Zhi Liu¹ · Xin Ge¹ · Bing-Hua Jiang¹ · Katherine Gibson-Corley¹ · Aloysius Klingelhutz¹⁰ · Nguan Soon Tan^{4,11,12,13} · Yuwen Zhu¹⁴ · Fayyaz S. Sutterwala¹⁵ · Xian Shen¹⁶ · Weizhou Zhang^{1,2,3,5,6}

Received: 9 May 2018 / Revised: 18 September 2018 / Accepted: 13 November 2018 / Published online: 5 December 2018
© Springer Nature Limited 2018

Abstract

Obesity is a risk factor for breast cancer and also predicts poor clinical outcomes regardless of menopausal status. Contributing to the poor clinical outcomes is the suboptimal efficacy of standard therapies due to dose limiting toxicities and obesity-related complications, highlighting the need to develop novel therapeutic approaches for treating obese patients. We recently found that obesity leads to an increase in tumor-infiltrating macrophages with activated NLRC4 inflammasome and increased interleukin (IL)-1 β production. IL-1 β , in turn, leads to increased angiogenesis and cancer progression. Using Next Generation RNA sequencing, we identified an NLRC4/IL-1 β -dependent upregulation of angiopoietin-like 4 (ANGPTL4), a known angiogenic factor in cancer, in tumors from obese mice. ANGPTL4-deficiency by genetic knockout or treatment with a neutralizing antibody led to a significant reduction in obesity-induced angiogenesis and tumor growth. At a mechanistic level, ANGPTL4 expression is induced by IL-1 β from primary adipocytes in a manner dependent on NF- κ B- and MAP kinase-activation, which is further enhanced by hypoxia. This report shows that adipocyte-derived ANGPTL4 drives disease progression under obese conditions and is a potential therapeutic target for treating obese breast cancer patients.

Introduction

Obesity is associated with an increased risk of estrogen receptor-positive breast cancer in postmenopausal women and a worse clinical outcome regardless of menopausal status [1]. While outcomes for obese patients are worse, treatment options are the same despite often being less efficacious due to dose-limiting toxicities and obesity-related complications, thus underlying the need to develop specific therapies for better treating obese patients. We

recently found that obesity promotes breast cancer progression by inducing the activation of NLRC4 inflammasome and the consequent IL-1 β production from macrophages. IL-1 β then promotes angiogenesis and disease progression [2]. An association between obesity and increased tumor angiogenesis has been reported in several other studies [3–5], underscoring the potential importance of increased angiogenesis to obesity-driven breast cancer progression.

Antiangiogenic therapies have been approved for use in several types of cancer; however, survival benefits have been minimal [6]. In breast cancer, the anti-vascular endothelial growth factor (VEGF) antibody, bevacizumab, failed approval following phase 3 clinical trials due to a lack of overall survival benefits [7]. Thus, identifying patients who may benefit from anti-angiogenic therapies and understanding mechanisms of resistance is important. Studies have shown that anti-VEGF therapies may be beneficial in breast cancer patients with high levels of vascular density. Obese breast cancer patients may represent one such cohort that may respond to anti-angiogenic therapies. However, obesity may promote resistance to anti-VEGF therapy [8].

Electronic supplementary material The online version of this article (<https://doi.org/10.1038/s41388-018-0592-6>) contains supplementary material, which is available to authorized users.

- ✉ Ryan Kolb
ryankolb@ufl.edu
- ✉ Xian Shen
shenxian1120@126.com
- ✉ Weizhou Zhang
zhangw@ufl.edu

Extended author information available on the last page of the article

Angiopoietin-like 4 (ANGPTL4) is a secreted protein that is cleaved into two active peptides [9]. The N-terminus domain is a potent inhibitor of lipoprotein lipase (LPL) activity and modulates lipid composition and energy homeostasis [9]. The C-terminus (cANGPTL4) domain is involved in wound healing, vessel permeability, and angiogenesis [10]. ANGPTL4 plays a role in promoting the progression of several types of cancer [11, 12] and is correlated with poor response to anti-VEGF therapy [13]. Here we show that obesity-associated NLRC4 inflammasome activation/IL-1 β leads to the upregulation of ANGPTL4, primarily in adipocytes. This increase in ANGPTL4 is required for obesity-driven breast cancer progression and angiogenesis and targeting cANGPTL4 with a neutralizing antibody inhibits obesity-driven tumor progression.

Results

Obesity-associated NLRC4-inflammasome activation/IL-1 β upregulates *Angptl4*

We recently found that obesity promotes breast cancer progression via NLRC4-inflammasome activation and subsequent IL-1 β secretion in tumor-infiltrating macrophages [2]. To further understand how NLRC4-inflammasome promotes cancer progression, we performed Next Generation RNA sequencing on Py8119 orthotopic tumors from wild-type (wt) mice given a normal diet (ND), WT mice with high-fat diet (HFD), or the HFD-fed *Nlrc4*^{-/-} mice used in our previous study [2]. Using the criterion described in the materials and methods, we identified 8 genes that

were upregulated in an NLRC4-dependent manner in tumors from obese mice and 10 that were downregulated (Fig. 1a). Among the most highly upregulated genes was *Angptl4*, whose expression was further verified by real-time PCR showing an increase in Py8119 (Fig. 1b) and E0771 (Fig. 1c) mammary tumors from obese mice but not in those from obese NLRC4 inflammasome-deficient mice (*Nlrc4*^{-/-} HFD and *Casp1/11*^{-/-} HFD, the common effector enzyme for inflammasomes).

ANGPTL4 promotes obesity-driven breast cancer progression and angiogenesis

To determine if ANGPTL4 plays a role in obesity-driven breast cancer progression, we fed *Angptl4*^{-/-} and *Angptl4*^{+/-} littermates an ND or HFD for 10 weeks prior to implantation of Py8119 cells. We observed no significant difference in weight gain between the *Angptl4*^{-/-} and *Angptl4*^{+/-} mice (Fig. 2a). Tumor growth in *Angptl4*^{+/-} mice fed with the HFD was significantly higher than that in *Angptl4*^{-/-} mice fed with ND (Fig. 2b). This obesity-driven tumor progression was significantly reduced in *Angptl4*^{-/-} mice (Fig. 2b). Tumor growth in *Angptl4*^{-/-} mice fed HFD was similar to that of *Angptl4*^{+/-} and *Angptl4*^{-/-} mice fed ND, suggesting that only in the obese setting is tumor growth dependent on ANGPTL4. We next verified the role of ANGPTL4 in obesity-driven breast cancer progression using E0771 breast cancer cells and found similar results (Fig. 2c). Obesity led to an increase in tumor growth in WT mice and was partially, but significantly reduced ($P = 0.016$) in obese *Angptl4*-deficient mice (Fig. 2c). These data support that the upregulation of ANGPTL4 is critical in promoting cancer progression under obesity.

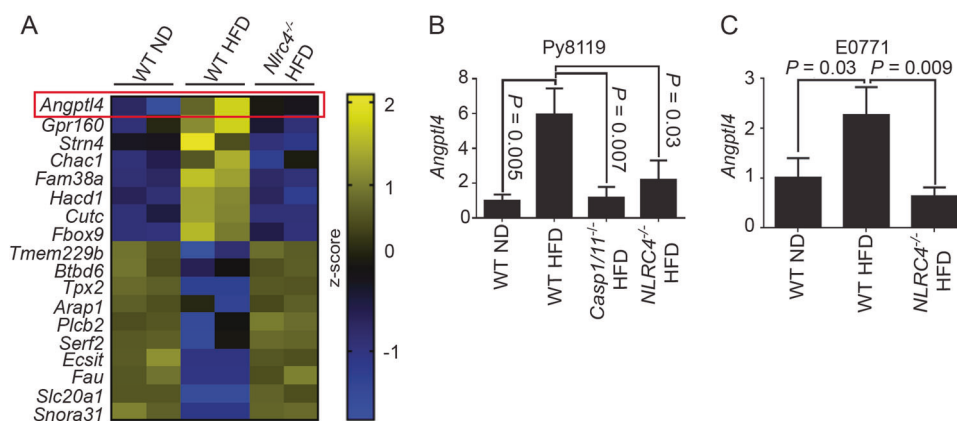


Fig. 1 NLRC4-inflammasome upregulates ANGPTL4 in tumors from diet-induced obese mice. **a** Heatmap showing differentially regulated genes in tumors from diet-induced obese mice that are NLRC4-dependent. Next generation RNA sequencing was performed using tumor RNAs from WT mice fed a normal diet (WT ND), WT mice fed a high-fat diet (WT HFD), or *Nlrc4*^{-/-} mice fed a HFD (*Nlrc4*^{-/-}

HFD). Each lane represents a combination of equal amount of RNAs from 3 individual tumors. **b, c** Average *Angptl4* mRNA relative to *Ppia* in tumors from the indicated mice presented as a fold change compared to WT ND. ($n = 3$ for all groups). One-way ANOVA with multiple comparisons correction using Dunnett's test was performed to determine significance in **b, c**

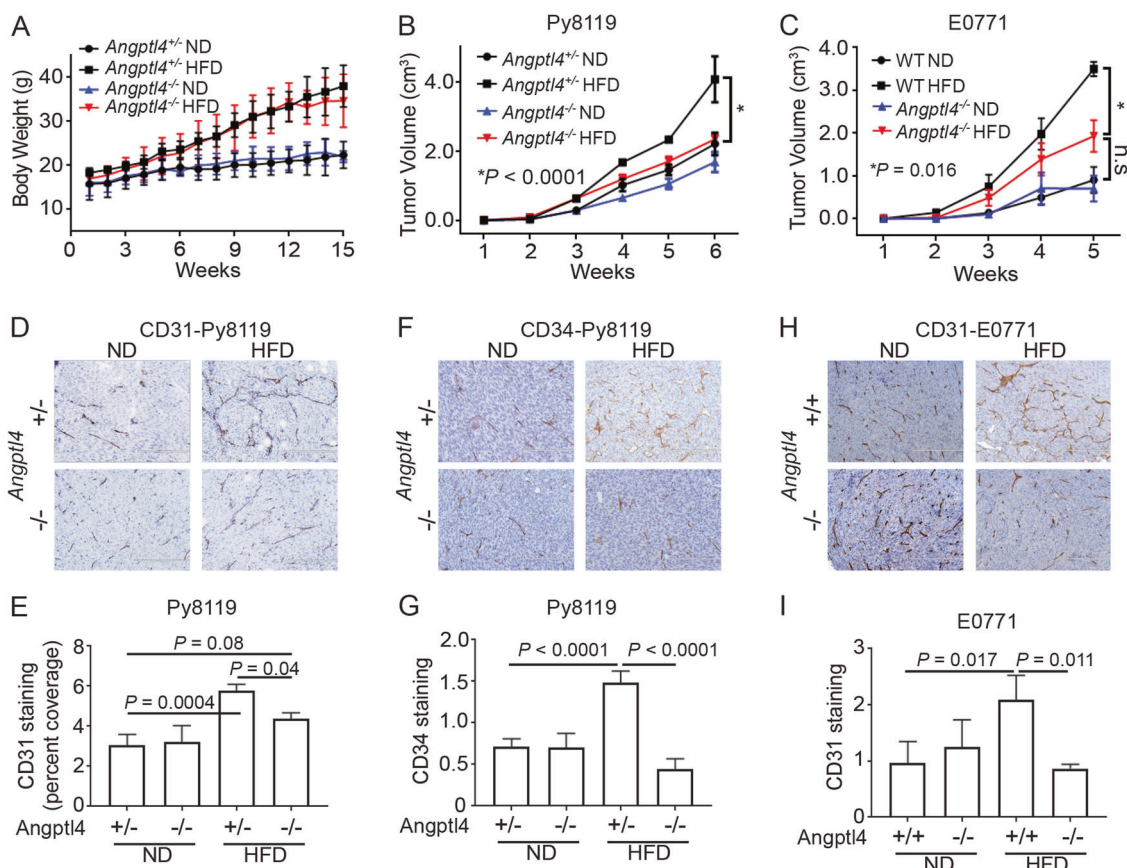


Fig. 2 ANGPTL4 promotes tumor growth and angiogenesis in obese mice. **a, b** *Angptl4*^{+/-} and *Angptl4*^{-/-} littermates were fed either a normal diet (ND) or high-fat diet (HFD) for 10 weeks, followed by implantation of 1×10^5 Py8119 cells into the #4 mammary fatpad. Graphs depict the average body weight \pm s.e.m. (**a**) and tumor volumes (**b**) \pm s.e.m. from the indicated mice ($n = 5$ *Angptl4*^{-/-} ND; $n = 6$ *Angptl4*^{-/-} HFD; $n = 6$ *Angptl4*^{+/-} ND; $n = 8$ *Angptl4*^{+/-} HFD). **c** The indicated mice were given an ND or HFD for 10 weeks and then implanted with 1×10^5 E0771 cells. Graph depicts the average tumor volumes \pm s.e.m. for the indicated mice ($n = 5$ for all groups). **d, e** IHC staining of CD31 from tumors used in Fig. 2b. **d** Representative images from the indicated mice. Scale bars: 200 μ m. **e** Average CD31-positive \pm s.d. staining as a percent of total pixels in tumors from the

indicated mice (At least 4 fields per sample and 3 samples per group were quantified). **f, g** IHC staining of CD34 from tumors used in Fig. 2b. **f** Representative images from the indicated mice. Scale bars: 200 μ m. **g** Average CD34-positive \pm s.d. staining in tumors from the indicated mice (At least 4 fields per sample and 3 samples per group were quantified). **h, i** IHC staining of CD31 from tumors used in Fig. 2c. **h** Representative images from the indicated mice. Scale bars: 200 μ m. **i** Average CD31-positive \pm s.d. staining in tumors from the indicated mice (At least 4 fields per sample and 3 samples per group were quantified). Two-way ANOVA was used to determine significance in **a–c**. One-way ANOVA with multiple comparisons correction using Dunnett's test was performed to determine significance in **e, g**, and **i**

It has been previously reported that *Angptl4*^{-/-} mice given a diet high in saturated fatty acids, such as the one used in our studies, have a systemic inflammatory response eventually leading to intestinal fibrosis and cachexia [14]. The authors noted that *Angptl4*^{-/-} mice given a diet high in unsaturated fatty acids did not present any of these clinical abnormalities. To determine if this inflammatory response may effect tumor growth in our model, we fed WT and *Angptl4*^{-/-} mice a safflower oil-based HFD consisting of primarily 18:2 unsaturated fatty acids (HFD-Saff); however, the *Angptl4*^{-/-} mice failed to gain weight making this an inappropriate model to study obesity-driven breast cancer progression (Supplementary Figure S1a). This lack of weight gain from 18:2 unsaturated fatty acids is an intriguing future avenue of investigation for the role of

ANGPTL4 in the regulation of LPL. Furthermore, tumors from *Angptl4*^{-/-} mice given a HFD had similar numbers of tumor-infiltrating macrophages and IL-1 β levels as those in *Angptl4*^{+/-} mice (Supplementary Figure S1b-d).

In our previous study, we found that NLRC4-inflammasome promotes tumor angiogenesis in obese mice [2]. As previous studies have shown that ANGPTL4 can promote angiogenesis [15], we next determined if upregulation of ANGPTL4 in obese mice led to increased angiogenesis. Immunohistochemical staining for CD31, a marker for endothelial cells, showed a significant increase in CD31-positive staining in tumors from *Angptl4*^{+/-} HFD mice compared to *Angptl4*^{+/-} ND mice (Fig. 2d, e). This increase in CD31-positive staining was partially reduced in *Angptl4*^{-/-} HFD mice, suggesting that obesity-driven tumor

angiogenesis is at least partially dependent on ANGPTL4. While obese *Angptl4*^{-/-} mice had increased CD31 staining compared to *Angptl4*^{+/-} or *Angptl4*^{-/-} ND mice, the difference was not significant (Fig. 2d, e). Similar results were found using a second endothelial cell marker, CD34, wherein tumors from obese wild-type mice had increased CD34-positive staining compared to ND mice but not in those from obese ANGPTL4-deficient mice (Fig. 2f, g). In Fig. 2d–g, the tumors were collected at the same time and hence the tumors from the HFD group were larger (Fig. 2b). To determine if this difference in size played a role in the increased angiogenesis, we collected tumors from ND and HFD mice when they reached 2 cm in diameter and stained for CD31. Tumors from obese mice still had increased CD31 staining compared to tumors from ND mice, indicating that the difference in angiogenesis was not due to the larger tumors (Supplementary Figure S2a). This ANGPTL4-dependent increase in angiogenesis was also seen in E0771 tumors (Fig. 2h, i), further supporting the role of obesity-associated ANGPTL4 in promoting tumor angiogenesis. We also stained tumor sections for Ki-67, a proliferation marker, and found no difference between tumors from obese and ND mice (Supplementary Figure S2 b).

IL-1 β promotes the upregulation of *Angptl4* in adipocytes

To determine the source of ANGPTL4 in response to IL-1 β in obese tumor, we treated various cell types found in the tumor microenvironment with IL-1 β and measured *Angptl4* expression. IL-1 β did not induce *Angptl4* expression in Py8119 cancer cells, bone-marrow-derived macrophages (BMDM, M ϕ), cancer-associated fibroblasts (CAFs), or endothelial cells (SVEC; Fig. 3a). In contrast, IL-1 β induced a significant, 28-fold increase in *Angptl4* mRNA in primary mouse adipocytes (Fig. 3a). It should also be noted that the relative expression of *Angptl4* is 200x or higher in primary adipocytes than in the other cell types tested (Fig. 3a). The high expression of *Angptl4* in mouse adipocytes corresponds with RNA-sequencing data from human tissues showing that adipose tissue has the highest expression of *ANGPTL4* (Supplementary Figure S3a). Western Blotting analysis of whole cell lysates and media from human adipocytes, obtained by differentiation of an immortalized preadipocyte cell line [16], showed that IL-1 β induced ANGPTL4 protein in human adipocytes mainly as the secreted form in media (Fig. 3b). Adipocytes are an important cell type in the breast tumor microenvironment [17] and are frequently found in mammary tumors. The number of adipocytes was increased in tumors from obese mice regardless of whether ANGPTL4 was present (Supplementary Figure S3b–c). The high expression of

ANGPTL4 in primary adipocytes compared to other stromal cells indicates that ANGPTL4 is primarily produced from adipocytes in the obese microenvironment. To determine which signaling pathway is involved in the upregulation of *Angptl4*, we treated adipocytes with IL-1 β in the presence or absence of either an NF- κ B- or a JNK-inhibitor. Inhibition of NF- κ B partially reduced IL-1 β -induced upregulation of *Angptl4* expression in primary adipocytes, while inhibition of JNK attenuated IL-1 β -induced *Angptl4* (Fig. 3c), suggesting that ANGPTL4 expression is induced through NF- κ B- and JNK-mediated signaling pathways. We also treated primary mouse adipocytes with IL-1 β in the presence or absence of D-JNKi, a cell-permeable peptide inhibitor of JNK [18], or control peptide and confirmed that inhibition of JNK signaling abolished IL-1 β -induced *Angptl4* (Fig. 3d). The inhibition of IL-1 β -induced JNK activation was confirmed by Western Blotting for phospho-c-JUN downstream of JNK activation (Supplementary Figure 3d). We transduced differentiated human adipocytes with adenovirus expressing GFP (Ad-GFP), dominant-negative (DN) JNK (Ad-DN-JNK) or DN IKK β (Ad-DN-IKK β), following with IL-1 β treatment. Infectivity was verified by expression of GFP (Supplementary Figure S3e). IL-1 β -induced expression of *ANGPTL4* in human adipocytes was inhibited by the expression of DN JNK and DN IKK β (Fig. 3e), further confirming the role of NF- κ B- and JNK-mediated signaling in the regulation of ANGPTL4 downstream of IL-1 β .

ANGPTL4 is known to be regulated by hypoxia-inducible factor 1 (HIF1) [19]. We stained tumor sections with HIF1 α and counted the number of cells with nuclear HIF1 α staining as a marker for hypoxia. While we didn't see an increase in nuclear HIF1 α staining in tumors from obese mice, both the tumor microenvironment and obese adipose tissues tend to have regional hypoxia (Supplementary Figure S3f–g). We hence determined the effect of hypoxia on IL-1 β -induced *Angptl4*. While both hypoxia (incubation of cells at 1% O₂) and IL-1 β induced the expression of *Angptl4*, the combination of IL-1 β and hypoxia induced a further upregulation of *Angptl4* relative to either alone: 4.7-fold increase over hypoxia alone and 11.1-fold increase over IL-1 β alone (Fig. 3f). Human adipocytes were treated as in Fig. 3f and similar to mouse adipocytes, hypoxia induced a significant increase in *ANGPTL4* expression, which is further increased by IL-1 β (Fig. 3g). We previously showed that vascular endothelial growth factor (VEGF) A is upregulated by IL-1 β in obese tumors in our model [2]. As such, we examined the IL-1 β induced *Vegfa* in adipocytes in conjunction with hypoxia. In primary adipocytes, while both IL-1 β and hypoxia induced *Vegfa* expression individually, the combination did not significantly increase its expression compared to hypoxia alone (Supplementary Figure S3h). These data indicate that

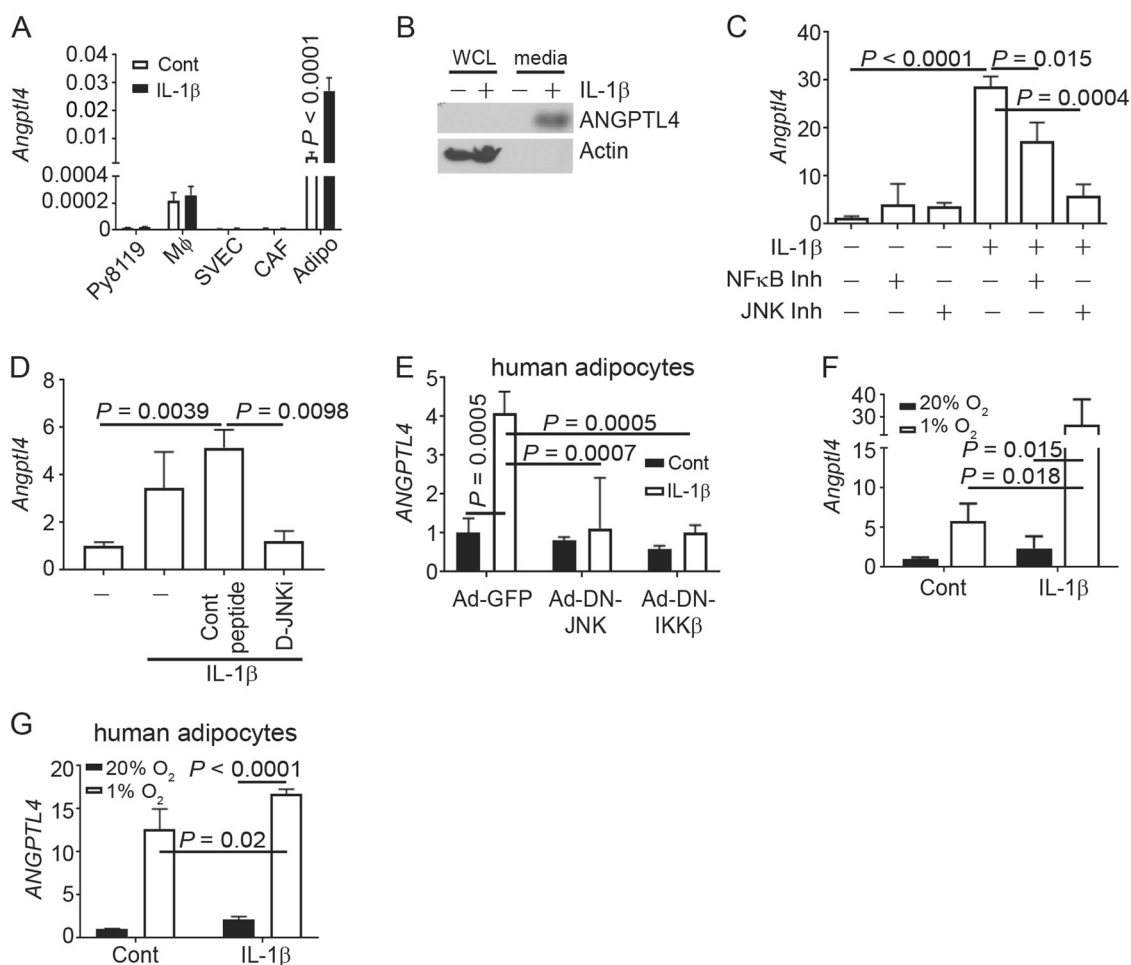


Fig. 3 IL-1 β directly upregulates ANGPTL4 in adipocytes. **a** The indicated cells were treated with 100 ng/ml IL-1 β for 6 h. Graph depicts the average *Angptl4* mRNA relative to *Ppia* \pm s.d. ($n = 3$ for all groups). **b** Human preadipocytes were differentiated into adipocytes and treated with 100 ng/ml of IL-1 β for 4 h. Then the media was collected and cells were lysed. Immunoblots for ANGPTL4 is shown. β -ACTIN was included as a loading control. **c** Primary mouse adipocytes were treated as indicated. Graph depicts the average *Angptl4* mRNA relative to *Ppia* \pm s.d. as a fold change compared to control ($n = 3$ for all groups). **d** Primary mouse adipocytes were treated with 30 μ M D-JNKi or control peptide 1 h prior to treatment with 100 ng/ml IL-1 β for 6 h. Graph depicts the average *Angptl4* mRNA relative to *Ppia* \pm s.d. ($n = 3$ for all groups). **e** Differentiated human adipocytes were transduced with adenovirus expressing GFP (Ad-GFP), dominant-negative JNK (Ad-DN-JNK) or dominant-negative IKK β

(Ad-DN-IKK β) for 16 h then treated with 100 ng/ml IL-1 β for 6 h. Graph depicts the average *ANGPTL4* mRNA relative to *ACTB* \pm s.d. ($n = 3$ for all groups). **f** Primary adipocytes were treated with or without IL-1 β and incubated at 20% or 1% O $_2$ for 6 h. Graph depicts the average *Angptl4* mRNA relative to *Ppia* \pm s.d. as a fold change compared to control ($n = 3$ for all groups). **g** Immortalized human preadipocytes were differentiated into mature adipocytes then treated as in **c**. Graph depicts the average *ANGPTL4* mRNA relative to *PPIA* \pm s.d. as a fold-change compared to control ($n = 3$ for all groups). In (**c**, **d**, **f**) data depicts the results of a single experiment using adipocytes from one litter of mice treated in triplicate. Experiments were repeated using different batches of adipocytes with similar results. One-way ANOVA with multiple comparisons correction using Dunnett's test was performed to determine significance

the upregulation of IL-1 β in obese tumors acts collectively with hypoxia to induce *Angptl4* expression in adipocytes.

ANGPTL4 in human obesity and breast cancer

We next examined the relevance of ANGPTL4 in human obesity and breast cancer. Analysis of the publicly available dataset (GSE33256) showed a significant increase in the expression of *ANGPTL4* in normal breast tissue from obese women compared to normal weight women (Fig. 4a). Using a meta-dataset with 2315 samples, we found that *ANGPTL4*

expression was inversely correlated with recurrence-free survival (RFS; hazard ratio HR = 1.3) across all breast cancer subtypes (Fig. 4b), which became much more pronounced within basal-like breast cancer (HR = 2.05; Fig. 4c). Examining TCGA breast cancer expression data, we also found that *ANGPTL4* expression was highest in aggressive basal-like breast cancer compared to Luminal A, Luminal B, and HER2 subtypes (Fig. 4d).

We analyzed basal-like breast cancers as they had the highest expression of *ANGPTL4*, and found that there is a positive correlation between *ANGPTL4* and *PECAMI1*

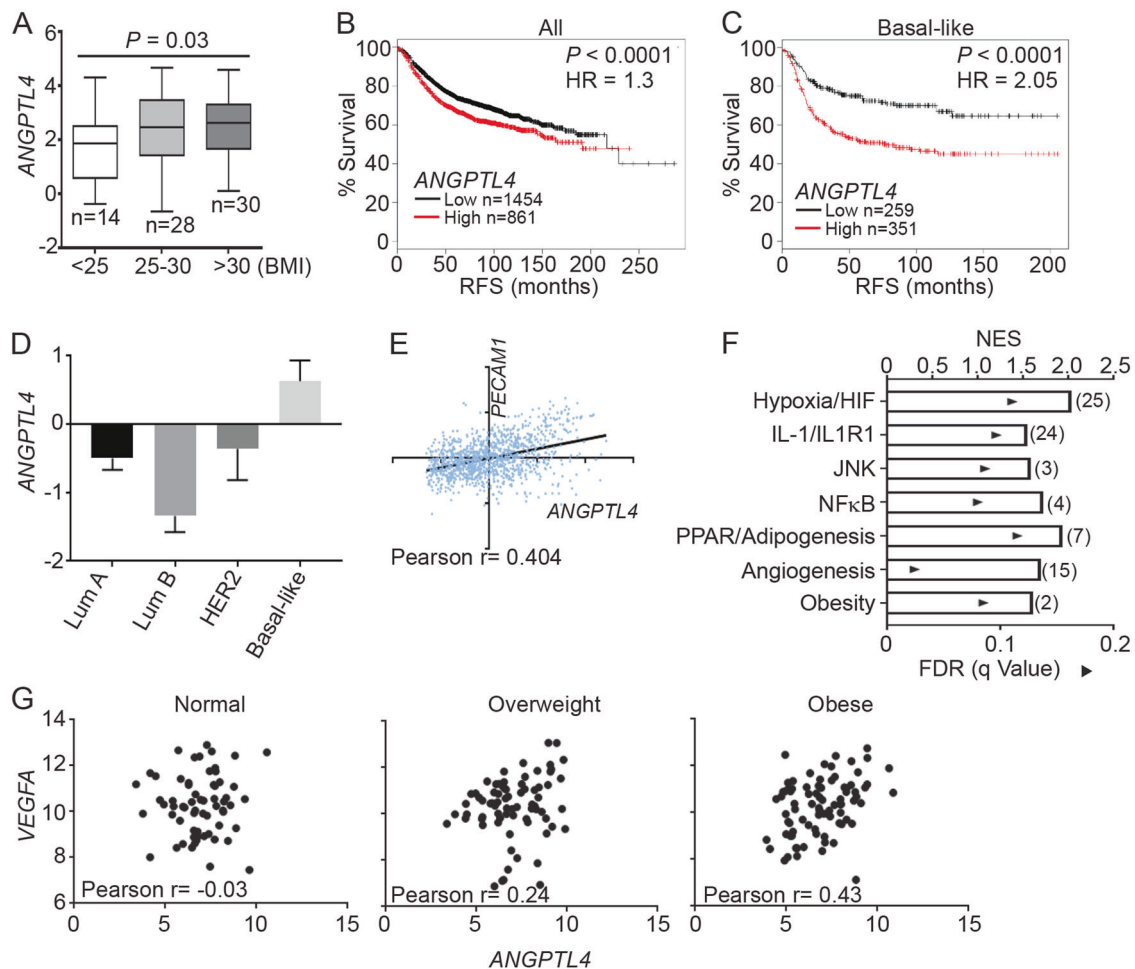


Fig. 4 ANGPTL4 in human obesity and breast cancer. **a** Box plots depicting *ANGPTL4* mRNA with 95% confidence interval (CI) in normal mammary tissue in normal weight (BMI <25), overweight (BMI 25–30) and obese (BMI >30) patients. Data were from GSE33256. Number of samples is indicated. Welch's *t* test was used to determine significance. **b, c** Correlation between *ANGPTL4* mRNA and recurrence-free survival (RFS) in all breast cancer samples (**b**) and basal-like breast cancer **c**. Data generated using KMplot meta-dataset of invasive ductal breast carcinoma. Number of cases and Log-rank *P* values are shown. **d** Mean centralized *ANGPTL4* mRNA with 95% CI in PAM50 subtypes of breast cancer. Data from TCGA invasive breast cancer cohort. **e** Correlation between *ANGPTL4* and *PECAM1* mRNA in basal-like breast cancers. Data is from the basal-like breast cancer

subtype of the TCGA invasive breast cancer cohort. Pearson *r* is indicated. **f** Gene Set Enrichment Analysis of basal-like breast cancer samples comparing *ANGPTL4* high expression tertile ($n=66$) to *ANGPTL4* low expression tertile ($n=66$) from GEO data sets GSE76275. Graph depicts the nominal enrichment score (NES; bar) and FDRs (solid triangles) of a representative gene set related to the indicated pathway enriched in the *ANGPTL4* high tertile group. The number of pathways enriched related to the indicated pathways is labeled in parenthesis. Only gene sets with FDRs <0.25 were considered significantly enriched. **g** Correlation between *VEGFA* and *ANGPTL4* mRNA in breast cancer samples from normal (BMI <25), overweight (BMI 25–30), and obese (BMI >30) patients from GSE20194. Pearson *r* is indicated

(CD31) (Fig. 4e), suggesting that *ANGPTL4* is positively correlated with angiogenesis in human breast cancer. Using a publicly available dataset of 198 basal-like breast cancer samples (GSE76275), we performed Gene Set Enrichment Analysis (GSEA) comparing transcriptomes with high expression of *ANGPTL4* vs. those with low expression of *ANGPTL4*, to identify pathways and gene sets associated with *ANGPTL4*. We found an enrichment for gene sets related to all of the *ANGPTL4* regulatory pathways, including those of hypoxia and HIF signaling, IL-1 signaling, JNK signaling, NF κ B signaling, and PPAR/Adipogenesis (Fig. 4f, Supplementary Table 1). We also found the

enrichment for gene sets related to angiogenesis and obesity, further corroborating an association between *ANGPTL4*, obesity and angiogenesis in breast cancer (Fig. 4f, Supplementary Table 1). We previously reported an upregulation of *VEGFA* in response to NLRC4 inflammasome/IL-1 β [2]. We also determined if *VEGFA* was associated with enrichment for gene sets related to the same pathways associated with *ANGPTL4* expression. While high *VEGFA* expression was associated with fewer pathways overall compared to pathways altered in high *ANGPTL4* specimens, *VEGFA* expression was associated with enrichment for pathways related to Hypoxia/HIF signaling

as well as NF κ B and PPAR/adipogenesis, but not pathways related to JNK, IL-1 or obesity (Supplementary Figure S4a, Supplementary Table 2). As expected, cancer specimens with high expression of *VEGFA* exhibited enrichment for gene sets related to angiogenesis and *VEGFA* signaling (Supplementary Figure S4a, Supplementary Table 2). We also found that cancer specimens with high expression of *ANGPTL4* had enrichment for gene sets related to the same pathways, regardless of whether the samples were first separated into groups with high or low expression of *VEGFA* (Fig. 4f, Supplementary Figure S4b, Supplementary Tables 3–4), suggesting that expression of *ANGPTL4* is associated with these pathways independently of *VEGFA* expression. Previous studies have found that both *VEGFA* and *ANGPTL4* are required for angiogenesis [19] in certain situations and that high expression of *ANGPTL4* is correlated with poor response to anti-VEGF therapies [13]. Interestingly, we found a body-mass index (BMI)-dependent correlation pattern between *VEGFA* and *ANGPTL4*, with significant correlation between *VEGFA* and *ANGPTL4* expression (Pearson $r=0.43$) in obese breast cancer patients, a trend to positive correlation in overweight patients (Pearson $r=0.24$), and no correlation in normal weight patients (Fig. 4g). These analyses suggest that *ANGPTL4* and VEGF cooperatively promote angiogenesis in obese patients.

Targeting cANGPTL4 inhibits obesity-driven breast cancer progression

To see if targeting *ANGPTL4* would inhibit obesity-driven breast cancer progression, we used a neutralizing antibody against the C-terminus of *ANGPTL4* [20, 21]. Mice were given either a ND or HFD for 10 weeks then implanted with Py8119 cells as in Fig. 2. Once tumors were palpable, the mice were treated with the anti-cANGPTL4 blocking antibody or IgG as a control (Fig. 5a). Blocking cANGPTL4 reduced obesity-driven tumor growth compared to obese mice treated with IgG control (Fig. 5a). Anti-cANGPTL4 antibody treatment in mice fed ND had no effect on tumor growth (Fig. 5a). Treating obese mice with anti-cANGPTL4 antibody also reduced tumor angiogenesis indicated by CD31 IHC staining as compared to obese mice treated with IgG, though the difference was barely insignificant (Fig. 5b, c). This data indicates that targeting cANGPTL4 with a neutralizing antibody can inhibit obesity-driven breast cancer progression and angiogenesis.

We had 5 monoclonal antibodies against human cANGPTL4 developed which bound to both denatured and folded human cANGPTL4. To determine if these antibodies could block cANGPTL4 function, we performed an endothelial cell tube formation assay [22]. Treatment of endothelial cells with recombinant human cANGPTL4 induced

tube formation (Fig. 5d, e). cANGPTL4-induced tube formation was inhibited by co-treating cells with antibodies targeting human cANGPTL4 (Fig. 5d, e). Importantly, these antibodies did not inhibit serum-induced tube formation (Figure S5). We next performed an in vivo matrigel plug assay using hemoglobin as a readout for angiogenesis [23]. As shown in Fig. 5f, g, recombinant cANGPTL4 induced angiogenesis in a dose-dependent manner in matrigel plugs from athymic nude mice (Fig. 5f, middle two panels vs. control panel) and quantitated by hemoglobin protein expression (Fig. 5g, bar 1, 2, and 4). The cANGPTL4-induced angiogenesis in vivo was completely blocked by treatment with our new anti-cANGPTL4 antibody (Fig. 5f, right two panels vs. middle two panels) and further quantitated by hemoglobin protein expression (Fig. 5g, bar 3 vs. 2 and bar 5 vs. 4). These data indicate that cANGPTL4 can directly induce angiogenesis and can be blocked with anti-ANGPTL4 antibody against cANGPTL4.

Discussion

Previously we showed that obesity-associated NLRC4-inflammasome activation in infiltrating macrophages drove increases in angiogenesis and breast cancer progression [2], suggesting that obese breast cancer patients may represent a patient cohort that might benefit from *VEGFA* targeted therapy. Bevacizumab (Avastin) is an FDA-approved neutralizing antibody for human *VEGFA* to treat several solid cancers, but it failed in breast cancer due to lack of overall survival benefit. There is no doubt that angiogenesis is required for tumor growth and progression. Here we identified *ANGPTL4*, a different angiogenic factor, as critical for angiogenesis under obesity. Obesity is known to be associated with increased *VEGFA* expression and angiogenesis. As depicted (Supplementary Figure S6), we found a much more pronounced increase in *ANGPTL4* expression from adipocytes that can be regulated by several pathways: (1) (purple) IL-1 β produced by macrophages directly acts on adipocytes and induces *Angptl4* transcription via JNK and NF- κ B pathways; and (2) (blue) Hypoxia within tumor microenvironment and obesity synergizes with IL-1 β to induce *Angptl4* transcription likely via HIF1 α . These multifaceted *Angptl4* regulations further implicate its important role in tumor growth and progression under obesity. Our animal data further demonstrate the critical role of *ANGPTL4* in obesity-driven tumor angiogenesis and growth in two breast cancer models, suggesting that *ANGPTL4* is one of the major obesity-induced angiogenic factors downstream of NLRC4-inflammasome activation and IL-1 β release from macrophages.

Based on the expression pattern of *ANGPTL4* in human tissues (Supplementary Figure S3a) and the high expression

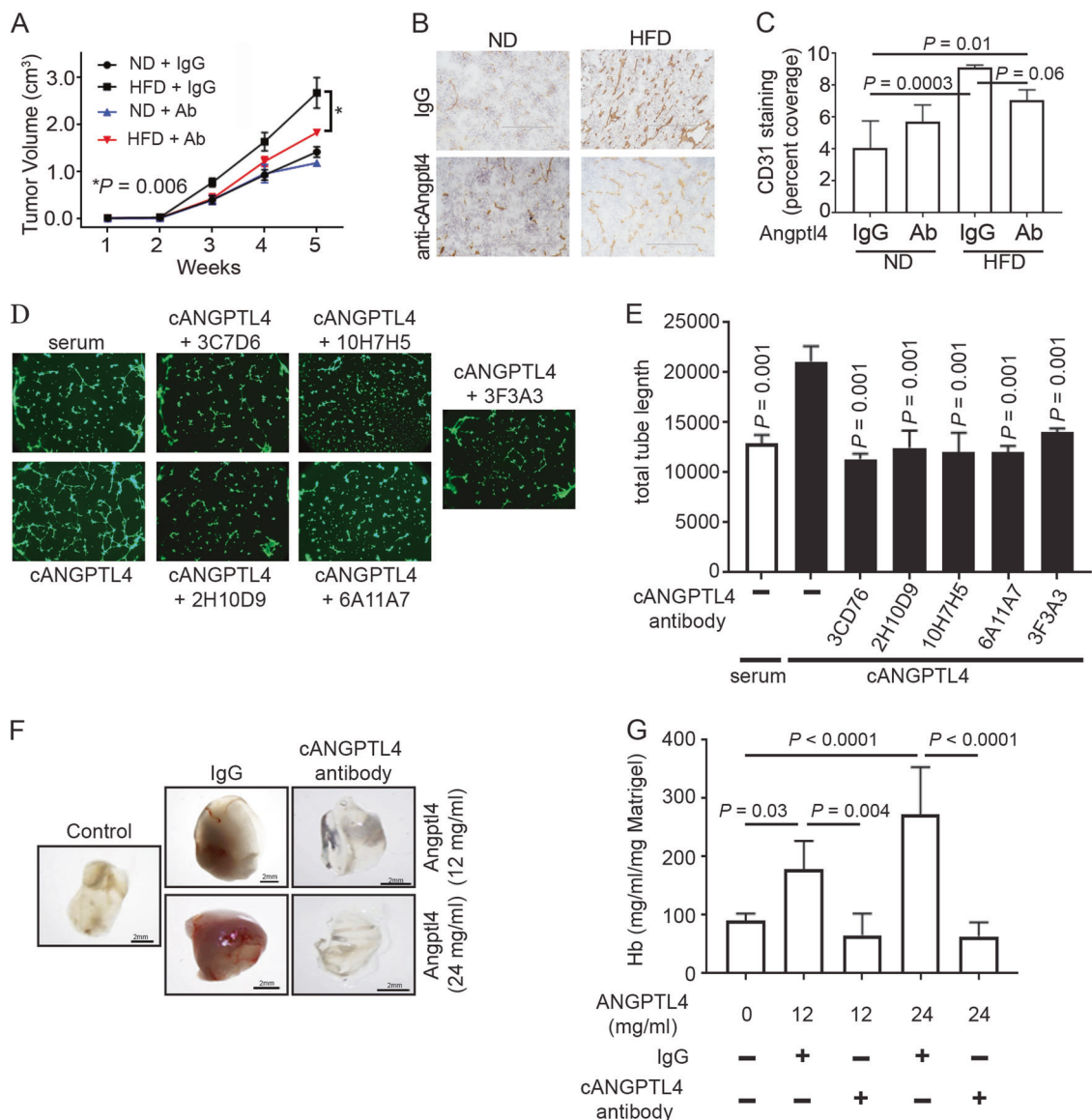


Fig. 5 Targeting cANGPTL4 inhibits obesity-driven cancer progression and angiogenesis. **a** WT mice were fed and implanted with Py8119 cells as described in Fig. 2. Mice were treated with anti-cANGPTL4 antibody (Ab) or rabbit IgG twice weekly once tumors were palpable. Graph depicts the average tumor volumes \pm s.e.m. from the indicated mice ($n = 5$ for all groups except ND IgG, $n = 4$). Two-way ANOVA was used to determine significance. **b**, **c** IHC staining for CD31 from tumors used in Fig. 5a. **b** Representative images from the indicated mice. Scale bars: 200 μ m. **c** Average CD31-positive staining \pm s.d. as a percent of total pixels in tumors from the indicated mice (At least 4 fields per sample and 3 samples per group were quantified). One-way ANOVA with multiple comparisons correction using Dunnett's test was performed to determine significance. **d**, **e** Endothelial

cell tube formation assay. Endothelial cells were plated on matrigel and treated as indicated. 6 h later cells were stained with Calcein AM and imaged (**d**). Images were analyzed and total tube length was determined. Graph (**e**) depicts the average total tube length \pm s.d. ($n = 3$ for all groups). One-way ANOVA with multiple comparisons correction using Dunnett's test was performed to determine significance. **f**, **g** Matrigel plug assay. Athymic nude mice were implanted with matrigel containing the indicated doses of recombinant human cANGPTL4 and 48 ng/ml anti-cANGPTL4 antibody or rat IgG. After 6 days, the matrigel plugs were removed and hemoglobin was measured as a readout for angiogenesis. Representative images (**f**) are shown. Graph (**g**) depicts the average hemoglobin concentration \pm s.d. ($n = 6$ for all groups)

of *Angptl4* in primary adipocytes compared to other stromal cells found in the tumor microenvironment (Fig. 3a), we hypothesize that adipocytes are the primary source of ANGPTL4 in the obese breast tumor microenvironment. Moreover, we observed a reduction in obesity-driven breast cancer progression when ANGPTL4 was lost in the

microenvironment but intact in the cancer cells (Fig. 2), indicating that the source of ANGPTL4 was from the tumor associated stroma. Previous studies have shown that cancer cells express ANGPTL4. In breast cancer, expression of TGF β can induce expression of *ANGPTL4*, which can promote lung metastasis [12]. Others have shown that

ANGPTL4 is expressed in various tumors and the loss of ANGPTL4 in squamous cell carcinoma and melanoma cells can reduce tumor growth in mouse models [24]. However, here we only focused on the relevance of stromal ANGPTL4 and our data indicate that the major source of ANGPTL4 in primary breast cancer under obesity could be adipocytes.

Our current focus is how the obesity-associated micro-environment promotes tumor growth and progression. Based on our and others' results, it is likely that hypertrophic adipocytes from obese individuals recruit macrophages via CCL2 production [5]. The activated macrophages produce IL-1 β via NLRC4-inflammasome activation, which in turn works on the above pathways to induce ANGPTL4 from adipocytes and consequent angiogenesis. Based on phenotypic resemblance between ANGPTL4-deficiency and NLRC4-inflammasome inactivation, we conclude that ANGPTL4 is the major downstream effector involved in obesity-driven tumor growth. As several mechanisms have been proposed, we reason that angiogenesis is one of the major pathways in the obesity-driven tumor growth as ANGPTL4 is critical in obesity-associated angiogenesis. We cannot exclude other pathways, but relevant to obesity in these models we did not find significant difference in apoptosis (data not shown) and proliferation (Supplementary Figure S2) between tumors from normal weight mice and those from obese mice. Several recent studies have found that ANGPTL4 can promote survival and proliferation of cancer cells through various mechanisms [24–27], providing possible mechanisms how ANGPTL4 promotes cancer progression that may be irrelevant of obesity. ANGPTL4-deficient mice have a systemic inflammatory response leading to intestinal fibrosis and cachexia when given a HFD that is high in saturated fatty acids, such as the one used in these studies, but not when given a HFD composed primarily of unsaturated fatty acids [14]. This inflammatory response may have an effect on tumor growth in our model. Since ANGPTL4-deficient mice failed to gain weight when given a safflower oil-based HFD consisting of primarily 18:2 unsaturated fatty acid (Supplementary Figure S1a), we cannot conclusively determine what effect, if any, this inflammatory response to a diet high in saturated fatty acids has on obesity-driven tumor growth in our model. However, we saw no difference in the number of tumor-infiltrating macrophages and IL-1 β between tumors from control HFD mice compared to *Angptl4*^{-/-} HFD mice (Supplementary Figure S1b-d). Furthermore, obesity-associated tumor growth was abrogated by treating mice with a neutralizing antibody targeting cANGPTL4 (Fig. 5a), suggesting that this inflammatory response in ANGPTL4-deficient mice was not responsible for the reduced tumor growth observed in obese *Angptl4*^{-/-} mice (Fig. 2b, c).

While anti-VEGF therapies have shown little therapeutic promise in breast cancer, they may be beneficial to patients with high levels of neoangiogenesis [28]. Due to the increase in angiogenesis in obesity-associated breast cancer, we have postulated that anti-VEGF therapies may be a viable therapy in obese breast-cancer patients [2]. However, a recent publication found that obesity promotes resistance to anti-VEGF therapies possibly through the upregulation of IL-6 and FGF-2⁸. Here we found that ANGPTL4 is required for obesity-driven breast cancer progression and angiogenesis, and that its expression is inversely correlated with relapse-free survival (Fig. 4). Moreover, we found that *VEGFA* and *ANGPTL4* expression are correlated only in obese patients (Fig. 4g). Previous studies have shown that expression of ANGPTL4 is correlated with poor response to anti-VEGFA therapies [13]. Thus, the upregulation of ANGPTL4 represents another mechanism for the resistance to anti-VEGF therapies in obese mice reported previously [8]. Therefore, targeting ANGPTL4 alone or in combination with anti-VEGF therapies may be a better potential therapy for obese breast cancer patients. In particular, the high expression in basal-like breast cancer and its secretory nature make ANGPTL4 an ideal target for antibody-based therapy. Indeed, treating mice with a neutralizing antibody against cANGPTL4 inhibits obesity-driven breast cancer progression in obese mice (Fig. 5a), further highlighting the potential of ANGPTL4 as a therapeutic target for obese breast cancer patients. One caveat is the critical role of its N-terminus in inhibiting LPL regulation that could be detrimental for lipid homeostasis if inhibited. It is unknown if antibodies targeting cANGPTL4 deplete the pool of whole length ANGPTL4 leading to a potential reduction of its N-terminal peptide. Further investigations are warranted to address if cANGPTL4 represents a viable target for therapy in particular to obese patients with basal-like breast cancer.

Materials and methods

Cell lines, primary adipocytes and cell culture

Py8119 and E0771 cells have been described and validated previously [2, 29, 30]. Cancer-associated fibroblast cells were described previously [31]. SVEC endothelial cells were purchased from American Type Culture Collection (ATCC) [32]. Cell lines were routinely tested for mycoplasma contamination. Human preadipocytes (Lonza, Basel Switzerland) were immortalized, cultured and differentiated into mature adipocytes as described previously [16]. Primary mouse preadipocytes were isolated from the mammary fat pad of 4 to 6-day-old pups and differentiated into mature adipocytes as described previously [33]. For experiments involving treatment with IL-1 β , cells were

cultured with 100 ng/ml recombinant mouse or human IL-1 β (R&D Systems, Minneapolis MN) for 6 h. For co-treatment with IL-1 β , adipocytes were treated with 5 μ M BMS345541 (Sigma-Aldrich, St. Louis, MO), an NF- κ B inhibitor, 40 μ M SP600125 (Sigma Aldrich) a JNK inhibitor, 30 μ M D-JNKi (GenScript, Piscataway NJ) or 30 μ M control peptide (GenScript), 1 h prior to treatment with IL-1 β . For transduction of differentiated human adipocytes, cells were incubated with purified adenovirus expressing GFP, DN JNK (University of Iowa Viral Vector Core) or DN IKK β for 16 h prior to treatment with IL-1 β . Each individual experiment involving primary adipocytes were performed using a batch of adipocytes from a single litter of mice plated in triplicate for each experimental group. These experiments were then repeated at least twice using different batches of primary adipocytes.

Mouse colony and orthotopic transplant model

Animal experiments were approved by the University of Iowa Institutional Animal Care and Use Committee (IACUC) and performed in accordance with IACUC guidelines. All mice used were female mice of C57BL/6N background. *Angptl4*^{-/-} (B6;129S5-Angptl4Gt (OST352973)Lex/Mmucd) mice were obtained from the Mutant Mouse Resource and Research Center (mmrrc.org) and backcrossed 10 generations with C57BL/6N background. For Py8119 transplant models, *Angptl4*^{+/-} and *Angptl4*^{-/-} littermates were used. Tumors from *Casp1/11*^{-/-} [34] and *Nlrc4*^{-/-} [35] mice were from our previous publication [2]. Athymic nude mice of both genders were purchased from Charles River Laboratories for matrigel plug assays (San Diego, CA).

The orthotopic transplant model was done as described previously [2]. Briefly, 6-week old mice were randomly grouped and given a normal diet provided by our vivarium, or a high-fat diet (HFD, 60% kCal from fat, S3282, Bio-Serv, Flemington, NJ) for 10 weeks, then Py8119 or E0771 cells in Matrigel/PBS were implanted into the #4 mammary gland. Experiments were terminated when the largest tumors reached 2 cm in diameter. A custom safflower oil-based HFD (60 kCal from fat) where in the fat content was 76.6% 18:2 fatty acid was obtained from Research Diets Inc. (New Brunswick, NJ). For experiments involving treatment of mice with antibody, mice were treated with 10 mg/kg anti-cANGPTL4 or rabbit IgG (BioXcell, West Lebanon, NH) twice weekly by intraperitoneal (*i.p.*) injection once tumors were palpable. The anti-cANGPTL4 antibody was described previously [20, 21]. For inbred mice, we expect to see variability representing $\leq 40\%$ of the mean of each group, thus, a minimum of 5 mice/group was used to exceed a confidence level of 95% for transplant models and repeated. Animal studies were not performed blinded due to the use of different diets and genotypes.

Western blotting and ELISA

For Western blotting analysis, adipocyte cells were lysed with RIPA buffer. Proteins in cell lysates or media were separated by SDS PAGE and detected by immunoblot analysis. The following antibodies were used: phospho-cJUN (K-M-1, Santa Cruz Biotechnologies, Dallas TX), rat anti-cANGPTL4 clone 6A11A7 (GenScript), and mouse anti- β -Actin (8H10D10, Cell Signaling Technology, Danvers MA). For ELISA, tissue was lysed in buffer consisting of 100 mM Tris pH 7.4, 150 mM NaCl, 1 mM ethylenediaminetetraacetic acid, 1 mM ethylene glycol-bis(β -aminoethoxy ether) N, N, N', N'-tetraacetic acid, 1% Triton X-100, and 0.5% sodium deoxycholate plus protease inhibitors. The ELISA was done using the following protein pair: rat anti-mouse IL-1 β (30311, R&D Systems, Minneapolis MN) and goat anti-mouse IL-1 β biotinylated (polyclonal, R&D). The ELISA was developed using TMB substrate (Thermo Fisher Scientific, Waltham MA).

Immunohistochemistry (IHC)

Tumor sections were preserved in OCT compound, frozen and sectioned. 5 μ m thick sections were fixed in 35/65 methanol/acetone. CD31 was detected with anti-mouse CD31 antibody (MEC13.3, Biolegend, San Diego CA). For the remaining IHC staining, Formalin-fixed tissue samples were paraffinized and sectioned by University of Iowa Comparative Pathology Core. Sections were then deparaffinized in a series of xylene washes and rehydrated with ethanol and water. Antigen retrieval was accomplished by immersing slides in Citrate Buffer pH 6.0 in a decloaker (Biocare Medical, Concord CA). Tissue samples were incubated with 3% hydrogen peroxide followed by blocking with horse serum (Biocare Medical). Slides were then incubated with rabbit anti-mouse Ki-67 antibody (D2H10, Cell Signaling Technology), rat anti-CD34 antibody (MEC14.7, Novus Biologicals, Littleton CO) or rabbit anti-HIF1 α (polyclonal, Abcam, Cambridge UK). Slides were then stained with Rat-on-mouse HRP polymer and probe (Biocare,) or secondary rabbit envision (DAKO, Santa Clara CA). The slides were developed with 3,3'-diaminobenzadine (DAB and 0.3% H₂O₂ in PBS) developing buffer, followed by counterstaining with hematoxylin. Positive staining was quantified using *Image J* software. All analysis of IHC was done blinded in regards to group allocation.

Endothelial cell tube formation assay

SVEC cells were serum-starved (0.3% serum) for 12 h, prior to plating 2×10^4 cells in DMEM in a growth factor reduced matrigel (Corning Inc., Corning NY) coated 48-well plate. 3% serum, recombinant human cANGPTL4

antibodies in hybridoma supernatant diluted 1:50 (GenScript, Piscataway NJ), and 20 µg/ml of cANGPTL4 was added to both the matrigel and the cell suspension as indicated. Rat anti-cANGPTL4 monoclonal antibodies were generated by GenScript against human cANGPTL4 protein. The ability of these proteins to bind to both denatured and folded cANGPTL4 was verified by GenScript by western blotting after SDS-PAGE and ELISA, respectively. Cells were then incubated for 6 h at 37 °C. Following incubation cells were stained with 2 µg/ml Calcein AM (Thermo Fisher Scientific) for 30 min followed by visualization using a fluorescent microscope. Tube formation was quantified using *AngioTool* software [36].

Matrigel plug assay

Athymic nude mice (Charles River Laboratories, San Diego, CA) were implanted with 0.4 ml growth factor reduced matrigel/PBS (Corning Inc.) containing the indicated concentration of recombinant human cANGPTL4 (Genescript) and 48 µg/ml rat IgG or purified rat anti-cANGPTL4 antibody clone 6A11A7 (Genescript) or PBS. After 6 days, mice were euthanized and plugs were used for the measurement of hemoglobin content using the Drabkin's reagent kit according to the manufacturer's instructions (Sigma-Aldrich). The concentration of hemoglobin was based on a set of standards.

Real-time PCR and RNA-seq

RNA was isolated using RNeasy Plus Mini Kit (Qiagen, Hilden, Germany). For real-time PCR, cDNA was generated using Superscript III First Strand cDNA Synthesis Kit (ThermoFisher Scientific). mRNA expression was quantified by real-time PCR using a ViiA7 Real-Time PCR System (ThermoFisher Scientific). The following primers for ANGPTL4 were used: for mouse, 5'-GGAAAAGTC-CACTGTGCCTC-3' and 5'-TAGATGACCCAGCT-GATTG-3'; for human 5'-TAGTCCCACTCTGCCTC TCCC-3' and 5'-GAGTTGGCCAGCCAGTT-3'. The following primers for mouse *Il1b* were used: 5'-GCAACTGTTCCCTGAACTCAACT-3' and 5'-ATCTT TTGGGGTCCGTCAACT-3'. For RNA-seq, samples were submitted to the Iowa Institute of Human Genomics for quality assessment and samples with a RNA Integrity Number score >8.0 were submitted to the University of Chicago Genomics for single-end 50 bp on the Illumina HiSeq 2000. Data was aligned using the Usegalaxy web platform and TopHat [37–39]. The aligned data was further processed using cufflinks workflow [40]. The raw data were shown as fragments per kilobase of transcript per million mapped reads (FPKM). Z-scores and fold change were calculated using the resulting expression data converted to

Log₂ (FPKM + 1) values. Due to the small sample size, 2 per group, determining statistical significance for differentially regulated genes was not possible. Instead, differentially regulated genes in tumors from obese that were NLRC4-dependent were identified as genes with a fold change of greater than or equal to |1.8|. The list was further narrowed to only genes that were upregulated in the HFD group and had a Z-score of greater than 0.5 while the Z-score for the other 4 samples (ND and *Nlrc4*^{-/-} HFD) were less than 0.25. For downregulated genes we included samples where the Z-score was less than 0.25 for the HFD samples and greater than 0.5 for the other 4. A heatmap of differentially regulated genes was made using Graphpad Prism Software (Graphpad Software Inc., San Diego, CA).

Survival and transcriptomics analysis

Recurrence-free survival based on the expression of *ANGPTL4* were generated using data from a published meta-dataset of 3554 breast cancer patient specimens and the KMplot online tools [41]. Expression analyses of the TCGA BRCA cohort were performed using the mean-centralized level 3 Illumina HiSeq2000 RNA-seq data separated into PAM50 subtypes. RNA-seq data from 122 human individual representing 32 tissues was obtained from Human Protein Atlas [42] and *ANGPTL4* expression in different tissues was graphed using Graphpad Prism Software (Graphpad Software Inc). Correlation between *ANGPTL4* and *PECAMI* mRNA was generated using Graphpad Prism Software (Graphpad Software Inc) using TCGA BRCA expression data from basal-like PAM50 subtype. GSE33256, GSE20914 and GSE76275 microarray data were obtained from NCBI Geo Datasets. BMI data for GSE20914 was provided by Dr. Sai-Ching Yeung at MD Anderson Cancer Center. For pathway analysis, basal-like breast cancer samples from GSE76275 were separated into high and low expressing tertiles of *ANGPTL4* (probe 221009_s_at) or *VEGFA* (probe 210512_s_at). Further analysis was done by first separating the samples by *VEGFA* expression into high tertile or low tertile, then further separating each group into high and low *ANGPTL4* expressing tertiles. Geneset Enrichment Analysis (Broad Institute of MIT and Harvard, Boston) was used comparing low expressing tertiles to high expressing tertile for each group. Genesets with a false discovery rate (FDR) < 0.25 was considered significant enrichment.

Statistical analysis

All statistical tests are described in the figure legends. For animal models, statistical significance for body weight and tumor growth was determined by two-way ANOVA. Statistical significance in expression from human microarray or TCGA data were determined by a Welch's *t* test. Pearson *r*

is reported for correlation between the expression of two genes. Long-rank test was used to determine significance for survival curves. All other experiments used a one-way ANOVA with multiple comparisons correction using Dunnett's test to determine significance. *P* values of less than 0.05 were considered significant.

Data Availability:

The processed RNA-sequencing data shown as fragments per kilobase of transcript per million mapped reads (FPKM) and their original FASTQ files are currently being submitted to GEO data sets.

Acknowledgements We would like to thank the Comparative Histopathology Core in the Department of Pathology, University of Iowa for the processing of fixed tissue and CD31 immunohistochemistry. We thank Dr. Mikhail Kolonin (UT health science center at Houston) and Dr. Leslie Ellies (UCSD) for sharing E0771 and Py8119 cells, respectively.

Financial Support: RK: NIH T32 AI007260; WZ: NIH R01 grants CA200673 and CA203834, Oberley Award (National Cancer Institute Award P30CA086862) from Holden Comprehensive Cancer Center at the University of Iowa; NB: NIH F30 CA206255; AK: Mark Stinski Developmental Grant from the Department of Microbiology, University of Iowa; BD: NIH R01HL130146; NST: grant from Ministry of Education, Singapore (MOE2014-T2-1-012); FSS: NIH R01 AI118719.

Compliance with ethical standards

Conflict of interest The authors declare that they have no conflict of interest.

References

- Kolb R, Sutterwala FS, Zhang W. Obesity and cancer: inflammation bridges the two. *Curr Opin Pharmacol.* 2016;29:77–89.
- Kolb R, Phan L, Borchering N, Liu Y, Yuan F, Janowski AM, et al. Obesity-associated NLR4 inflammasome activation drives breast cancer progression. *Nat Commun.* 2016;7:13007.
- Gu JW, Young E, Patterson SG, Makey KL, Wells J, Huang M, et al. Postmenopausal obesity promotes tumor angiogenesis and breast cancer progression in mice. *Cancer Biol Ther.* 2011;11:910–7.
- Fukumura D, Incio J, Shankaraiah RC, Jain RK. Obesity and cancer: an angiogenic and inflammatory Link. *Microcirculation.* 2016;23:191–206.
- Arendt LM, McCreedy J, Keller PJ, Baker DD, Naber SP, Seewaldt V, et al. Obesity promotes breast cancer by CCL2-mediated macrophage recruitment and angiogenesis. *Cancer Res.* 2013;73:6080–93.
- Jain RK. Antiangiogenesis strategies revisited: from starving tumors to alleviating hypoxia. *Cancer Cell.* 2014;26:605–22.
- Lohmann AE, Chia S. Patients with metastatic breast cancer using bevacizumab as a treatment: is there still a role for it? *Curr Treat Options Oncol.* 2012;13:249–62.
- Incio J, Ligibel JA, McManus DT, Suboj P, Jung K, Kawaguchi K, et al. Obesity promotes resistance to anti-VEGF therapy in breast cancer by up-regulating IL-6 and potentially FGF-2. *Sci Transl Med.* 2018;10:eaag0945.
- Lei X, Shi F, Basu D, Huq A, Routhier S, Day R, et al. Proteolytic processing of angiotensin-like protein 4 by proprotein convertases modulates its inhibitory effects on lipoprotein lipase activity. *J Biol Chem.* 2011;286:15747–56.
- Zhu P, Goh YY, Chin HF, Kersten S, Tan NS. Angiotensin-like 4: a decade of research. *Biosci Rep.* 2012;32:211–9.
- Tan MJ, Teo Z, Sng MK, Zhu P, Tan NS. Emerging roles of angiotensin-like 4 in human cancer. *Mol Cancer Res.* 2012;10:677–88.
- Padua D, Zhang XH, Wang Q, Nadal C, Gerald WL, Gomis RR, et al. TGFβ primes breast tumors for lung metastasis seeding through angiotensin-like 4. *Cell.* 2008;133:66–77.
- Bai L, Wang F, Zhang DS, Li C, Jin Y, Wang DS, et al. A plasma cytokine and angiogenic factor (CAF) analysis for selection of bevacizumab therapy in patients with metastatic colorectal cancer. *Sci Rep.* 2015;5:17717.
- Lichtenstein L, Mattijssen F, de Wit NJ, Georgiadi A, Hooiveld GJ, van der Meer R, et al. Angptl4 protects against severe proinflammatory effects of saturated fat by inhibiting fatty acid uptake into mesenteric lymph node macrophages. *Cell Metab.* 2010;12:580–92.
- Gealekman O, Burkart A, Chouinard M, Nicoloso SM, Straubhaar J, Corvera S. Enhanced angiogenesis in obesity and in response to PPARγ activators through adipocyte VEGF and ANGPTL4 production. *Am J Physiol Endocrinol Metab.* 2008;295:E1056–64.
- Vu BG, Gourronc FA, Bernlohr DA, Schlievert PM, Klingelutz AJ. Staphylococcal superantigens stimulate immortalized human adipocytes to produce chemokines. *PLoS ONE.* 2013;8:e77988.
- Choi J, Cha YJ, Koo JS. Adipocyte biology in breast cancer: From silent bystander to active facilitator. *Prog Lipid Res.* 2018;69:11–20.
- Bonny C, Oberson A, Negri S, Sauser C, Schorderet DF. Cell-permeable peptide inhibitors of JNK: novel blockers of beta-cell death. *Diabetes.* 2001;50:77–82.
- Hu K, Babapoor-Farrokhran S, Rodrigues M, Deshpande M, Puchner B, Kashiwabuchi F, et al. Hypoxia-inducible factor 1 upregulation of both VEGF and ANGPTL4 is required to promote the angiogenic phenotype in uveal melanoma. *Oncotarget.* 2016;7:7816–28.
- Goh YY, Pal M, Chong HC, Zhu P, Tan MJ, Punugu L, et al. Angiotensin-like 4 interacts with integrins beta1 and beta5 to modulate keratinocyte migration. *Am J Pathol.* 2010;177:2791–803.
- Li L, Chong HC, Ng SY, Kwok KW, Teo Z, Tan EH, et al. Angiotensin-like 4 increases pulmonary tissue leakiness and damage during influenza pneumonia. *Cell Rep.* 2015;10:654–663.
- DeCicco-Skinner KL, Henry GH, Cataisson C, Tabib T, Gwilliam JC, Watson NJ, et al. Endothelial cell tube formation assay for the in vitro study of angiogenesis. *J Vis Exp.* 2014;91:e51312.
- Malinda KM. In vivo matrigel migration and angiogenesis assay. *Methods Mol Biol.* 2009;467:287–94.
- Li H, Ge C, Zhao F, Yan M, Hu C, Jia D, et al. Hypoxia-inducible factor 1 alpha-activated angiotensin-like protein 4 contributes to tumor metastasis via vascular cell adhesion molecule-1/integrin beta1 signaling in human hepatocellular carcinoma. *Hepatology.* 2011;54:910–9.
- Hata S, Nomura T, Iwasaki K, Sato R, Yamasaki M, Sato F, et al. Hypoxia-induced angiotensin-like protein 4 as a clinical biomarker and treatment target for human prostate cancer. *Oncol Rep.* 2017;38:120–8.
- Kim SH, Park YY, Kim SW, Lee JS, Wang D, DuBois RN. ANGPTL4 induction by prostaglandin E2 under hypoxic

- conditions promotes colorectal cancer progression. *Cancer Res.* 2011;71:7010–20.
27. Huang Z, Xie J, Lin S, Li S, Huang Z, Wang Y, et al. The downregulation of ANGPTL4 inhibits the migration and proliferation of tongue squamous cell carcinoma. *Arch Oral Biol.* 2016;71:144–9.
 28. Tolaney SM, Boucher Y, Duda DG, Martin JD, Seano G, Ancukiewicz M, et al. Role of vascular density and normalization in response to neoadjuvant bevacizumab and chemotherapy in breast cancer patients. *Proc Natl Acad Sci USA.* 2015;112:14325–30.
 29. Biswas T, Gu X, Yang J, Ellies LG, Sun LZ. Attenuation of TGF-beta signaling supports tumor progression of a mesenchymal-like mammary tumor cell line in a syngeneic murine model. *Cancer Lett.* 2014;346:129–38.
 30. Sugiura K, Stock CC. Studies in a tumor spectrum. I. Comparison of the action of methylbis (2-chloroethyl)amine and 3-bis(2-chloroethyl)aminomethyl-4-methoxymethyl-5-hydroxy-6-methylpyridine on the growth of a variety of mouse and rat tumors. *Cancer.* 1952;5:382–402.
 31. Tan W, Zhang W, Strasner A, Grivennikov S, Cheng JQ, Hoffman RM, et al. Tumour-infiltrating regulatory T cells stimulate mammary cancer metastasis through RANKL-RANK signalling. *Nature.* 2011;470:548–53.
 32. O'Connell KA, Eddin M. A mouse lymphoid endothelial cell line immortalized by simian virus 40 binds lymphocytes and retains functional characteristics of normal endothelial cells. *J Immunol.* 1990;144:521–5.
 33. Markan KR, Naber MC, Ameka MK, Anderegg MD, Mangelsdorf DJ, Kliewer SA, et al. Circulating FGF21 is liver derived and enhances glucose uptake during refeeding and overfeeding. *Diabetes.* 2014;63:4057–63.
 34. Kuida K, Lippke JA, Ku G, Harding MW, Livingston DJ, Su MS, et al. Altered cytokine export and apoptosis in mice deficient in interleukin-1 beta converting enzyme. *Science.* 1995;267:2000–3.
 35. Lara-Tejero M, Sutterwala FS, Ogura Y, Grant EP, Bertin J, Coyle AJ, et al. Role of the caspase-1 inflammasome in *Salmonella typhimurium* pathogenesis. *J Exp Med.* 2006;203:1407–12.
 36. Zudaire E, Gambardella L, Kurcz C, Vermeren S. A computational tool for quantitative analysis of vascular networks. *PLoS ONE.* 2011;6:e27385.
 37. Goecks J, Nekrutenko A, Taylor J, Galaxy T. Galaxy: a comprehensive approach for supporting accessible, reproducible, and transparent computational research in the life sciences. *Genome Biol.* 2010;11:R86.
 38. Blankenberg D, Von Kuster G, Coraor N, Ananda G, Lazarus R, Mangan M, et al. Galaxy: a web-based genome analysis tool for experimentalists. *Curr Protoc Mol Biol.* 2010;Chapter 19:11–21.
 39. Giardine B, Riemer C, Hardison RC, Burhans R, Elnitski L, Shah P, et al. Galaxy: a platform for interactive large-scale genome analysis. *Genome Res.* 2005;15:1451–5.
 40. Trapnell C, Roberts A, Goff L, Pertea G, Kim D, Kelley DR, et al. Differential gene and transcript expression analysis of RNA-seq experiments with TopHat and Cufflinks. *Nat Protoc.* 2012;7:562–78.
 41. Gyorffy B, Lanczky A, Eklund AC, Denkert C, Budczies J, Li Q, et al. An online survival analysis tool to rapidly assess the effect of 22,277 genes on breast cancer prognosis using microarray data of 1,809 patients. *Breast Cancer Res Treat.* 2010;123:725–31.
 42. Uhlen M, Fagerberg L, Hallstrom BM, Lindskog C, Oksvold P, Mardinoglu A, et al. Proteomics. Tissue-based map of the human proteome. *Science.* 2015;347:1260419.

Affiliations

Ryan Kolb^{1,2} · Paige Kluz^{1,3} · Zhen Wei Tan⁴ · Nicholas Borchering^{1,5,6} · Nicholas Bormann⁷ · Ajaykumar Vishwakarma^{1,6} · Louis Balczak⁸ · Pengcheng Zhu⁴ · Brandon SJ. Davies⁹ · Francoise Gourronc¹⁰ · Ling-Zhi Liu¹ · Xin Ge¹ · Bing-Hua Jiang¹ · Katherine Gibson-Corley¹ · Aloysius Klingelutz¹⁰ · Nguan Soon Tan^{4,11,12,13} · Yuwen Zhu¹⁴ · Fayyaz S. Sutterwala¹⁵ · Xian Shen¹⁶ · Weizhou Zhang^{1,2,3,5,6}

¹ Department of Pathology, University of Iowa Carver College of Medicine, Iowa City, IA 52242, USA

² Department of Pathology, Immunology and Laboratory Medicine, University of Florida, Gainesville, FL 32610, USA

³ Free Radical and Radiation Biology, University of Iowa Carver College of Medicine, Iowa City, IA 52242, USA

⁴ School of Biological Sciences, Nanyang Technological University, 60 Nanyang Drive, Singapore 637551, USA

⁵ Medical Scientist Training Program, University of Iowa Carver College of Medicine, Iowa City, IA 52242, USA

⁶ Cancer Biology Graduate Program, University of Iowa Carver College of Medicine, Iowa City, IA 52242, USA

⁷ Department of Psychiatry, University of Iowa Carver College of Medicine, Iowa City, IA 52242, USA

⁸ Interdisciplinary Neuroscience graduate program, University of Iowa Carver College of Medicine, Iowa City, IA 52242, USA

⁹ Department of Biochemistry, Fraternal Order of Eagles Diabetes

Research Center, and Obesity Research and Education Initiative, University of Iowa, Iowa City, IA 52242, USA

¹⁰ Department of Microbiology and Immunology, University of Iowa Carver College of Medicine, Iowa City, IA 52242, USA

¹¹ Lee Kong Chian School of Medicine, Nanyang Technological University, 50 Nanyang Drive, Singapore 639798, Singapore

¹² Institute of Molecular Cell Biology, 61 Biopolis Drive, Proteos, Agency for Science Technology & Research, Singapore 138673, USA

¹³ KK Research Centre, KK Women's and Children Hospital, 100 Bukit Timah Road, Singapore 229899, Singapore

¹⁴ Department of Surgery, University of Colorado, Denver/Anschutz Medical Campus, Aurora, CO 80045, USA

¹⁵ Department of Medicine, Cedars-Sinai Medical Center, Los Angeles, CA 90048, USA

¹⁶ Division of Gastrointestinal Surgery, the Second Affiliated Hospital of Wenzhou Medical University, Zhejiang 325035, China